Gloeobacter Rhodopsin, Limitation of Proton Pumping at High Electrochemical Load

Arend Vogt, Jonas Wietek, and Peter Hegemann*
Institute of Biology, Experimental Biophysics, Humboldt-Universität zu Berlin, Berlin, Germany

ABSTRACT We studied the photocurrents of a cyanobacterial rhodopsin *Gloeobacter violaceus* (GR) in *Xenopus laevis* oocytes and HEK-293 cells. This protein is a light-driven proton pump with striking similarities to marine proteorhodopsins, including the D121-H87 cluster of the retinal Schiff base counterion and a glutamate at position 132 that acts as a proton donor for chromophore reprotonation during the photocycle. Interestingly, at low extracellular pH_o and negative voltage, the proton flux inverted and directed inward. Using electrophysiological measurements of wild-type and mutant GR, we demonstrate that the electrochemical gradient limits outward-directed proton pumping and converts it into a purely passive proton influx. This conclusion contradicts the contemporary paradigm that at low pH, proteorhodopsins actively transport H^+ into cells. We identified E132 and S77 as key residues that allow inward directed diffusion. Substitution of E132 with aspartate or S77 with either alanine or cysteine abolished the inward-directed current almost completely. The proton influx is likely caused by the pK_a of E132 in GR, which is lower than that of other microbial ion pumping rhodopsins. The advantage of such a low pK_a is an acceleration of the photocycle and high pump turnover at high light intensities.

INTRODUCTION

Besides chlorophyll-dependent photosynthesis, nature uses retinal-dependent light-driven ion pumps to energize cells by direct sunlight. These pumps were originally discovered in Archaea of high salt epitopes, but were later also found in moderately halophilic Eubacteria, Proteobacteria (1), and some *Eucarya* (2,3). Most light-driven pumps transport protons from the cytoplasm to the extracellular space to generate an electrochemical gradient that drives secondary events such as ATP biosynthesis. The most prominent member of this family, bacteriorhodopsin (BR) of *Halobacterium salinarum*, has been thoroughly studied, mostly by spectroscopy and x-ray crystallography, over the past four decades. Unidirectional proton transport in BR is driven by conformational changes of the protein and by H^+-transfer reactions between selected residues within the intracellular and extracellular H^+-conducting trails. The conformational changes are accompanied by absorption changes during the photocycle and lead to the definition of defined photocycle intermediates (4,5). Electric processes and bioenergetic considerations of BR were revealed primarily by studies in proteoliposomes, and on purple membranes attached to black-lipid membranes (6–9). Later, BR was studied electrically in *Xenopus laevis* oocytes and human embryo kidney (HEK)-293 cells (10,11).

The results obtained were consistent with earlier measurements of intact cells (12) in the sense that BR from *H. salinarum* could transport protons against a maximal load of ~−285 mV. The molecular details, however, that limit H^+ pumping at opposing proton motive forces remained unknown or poorly understood. Spectroscopic studies on BR suggested that the photocycle changes substantially at low pH because Schiff base deprotonation is invisible at acidic conditions (13). In electrophysiological experiments on BR and *Acetetabularia* rhodopsin (AR), the pump current approached zero at a very negative voltage without leaking or inverting its direction at any experimental condition (3,10,11). In contrast, Béjà et al. (1) reported that the so-called Green Proteorhodopsin (GPR) isolated from the marine γ-proteobacterium EBAC31A08 switches the pump direction from outward to inward at low extracellular pH. The authors further concluded that the high pK_a (~7.5) of D97 serving as the negative counterion of the protonated retinal Schiff base (RSBH), corresponding to D85 with pK_a of only ~2.5 in BR, is the most critical feature for this bifunctional behavior (14,15). The authors argue that external acidic conditions protonate PR-D97, resulting in release of the Schiff base proton to the intracellular side upon M-state formation during the photocycle. However, the notion of GPR-mediated inward pumping has been challenged by experiments with vesicles composed of GPR-expressing *Escherichia coli* cells and proteoliposomes reconstituted with purified PR, in which inward-directed ion pumping was not observed at acidic pH conditions (16,17).

Moreover, studies of purified GPR in detergent demonstrated that, during the photocycle under acid conditions, species with a deprotonated Schiff base did not accumulate. More importantly, no charge movement was observed in electrical measurements of preoriented GPR in acrylamide gels (18,19).

Here we present results from an electrophysiological study of the proton-pumping rhodopsin from cyanobacteria

Submitted June 11, 2013, and accepted for publication August 28, 2013.

*Correspondence: hegemann@rz.hu-berlin.de

Areng Vogt and Jonas Wietek contributed equally to this work.

Editor: Joseph Mindell.

0006-3495/13/11/2055/9 $2.00

http://dx.doi.org/10.1016/j.bpj.2013.08.031

Gloeobacter violaceus PCC 7421 (20) expressed in *Xenopus laevis* oocytes and HEK-293 cells. Two-electrode voltage-clamp assays in oocytes and whole-cell measurements in HEK-293 cells demonstrate that, although proton pumping was directed outward under most conditions, it became inward under extracellular acidic conditions and the presence of a negative membrane voltage. This influx was visible when the inward-directed proton motive force exceeded −260 mV, suggesting that the proton influx was purely passive. We also demonstrate that the key residue for the observed passive proton influx is E132, which functions as the proton donor for the retinal Schiff base (RSB), and the adjacent position S77 (21). Substitution of these residues blocked leakage at the expense of a reduced photocycle speed.

We present a model that explains the bidirectional ion transport modes for *Gloeobacter* rhodopsin (GR). Moreover, due to the highly conserved D121-H87 cluster and E132, we propose a similar model for marine proteorhodopsins. Common features but also differences among GPR, BR, and GR will be discussed at a molecular level. The large photocurrents of GR in oocytes opened up the opportunity to study the voltage-dependent proton transport in microbial rhodopsins with (to our knowledge) so-far unrivaled precision.

MATERIALS AND METHODS

Cloning and site-directed mutagenesis

A full-length GR-coding DNA sequence (accession no. Q7NP59) was cloned via *Bam*HI/*Hin*dIII into the pGEMHE vector, which consists of a T7 promoter and polyadenylation site. For expression into HEK-293 cells, the GR coding DNA was cloned into the pECFP-N1 vector using *Hin*dIII/*Sac*II. Site-directed mutagenesis was performed using the QuikChange Kit (Agilent Technologies, Santa Clara, CA) according to the manufacturer's instructions.

Preparation of mRNA

Capped mRNA was synthesized in vitro from *Nhe*I-linearized pGEMHE plasmid (mMessage mMachine T7kit; Life Technologies, Carlsbad, CA) according to the manufacturer's protocol except for the following 15 μL reaction: 0.5 μg/μL mRNA, 5 μL 2×NTP/CAP, 1.5 μL 10× Reaction Buffer, 1 μL Enzyme Mix, and 7 μL H_2O.

Expression in *Xenopus laevis* oocytes

Oocytes were prepared from female *Xenopus laevis* as described previously in Tsunoda et al. (3). Single oocytes were injected with 28 ± 2 ng mRNA and incubated in Ringer solution supplemented with 5 μM all-*trans*-retinal (Sigma, St. Louis, MO). Photocurrents were measured 4–5 days after RNA injection.

Two-electrode voltage-clamp measurements

Two-electrode voltage-clamp data was acquired using pClamp10.1 (Molecular Devices, Eugene, OR) and a Turbo Tec-03X amplifier (NPI Electronic, Tamm, Germany). Microelectrodes were fabricated from borosilicate glass capillaries (1.50 mm O.D. and 1.17 mm I.D.) using a micropipette puller (model No. P-97; Sutter instruments, Novato, CA) filled with 3 M KCl. The resistances of microelectrodes were 0.5–1.5 MΩ. An XBO 75 W xenon lamp (Osram, Munich, Germany) served as a light source for current voltage ($I(E)$) measurements, and was controlled by an LS3 shutter (Vincent Associates UNIBLITZ, Rochester, NY). Different broadband filters, namely K50 and K55 (500 nm and 550 ± 25 nm; Optics Balzers, Balzers, Switzerland), were used to limit wavelengths. Action spectra were measured with a Polychrome II (Till Photonics, Munich, Germany) and were linearly normalized to the corresponding photon flux at each wavelength. The composition of extracellular buffer solutions was as follows: 100 mM NaCl, 1 mM $MgCl_2$, 0.1 mM $CaCl_2$, 5 mM MOPS (pH_o 6.0 and pH_o 7.5, adjusted with 1 M NMG), 5 mM Glycine (pH_o 9.0 and pH_o 10.0, adjusted with 1 M NMG), and 5 mM citric acid/Na-citrate (pH_o 3.8 and 5.0, adjusted with citric acid/Na-citrate).

Transfection and recording of HEK-293 cells

The cells were cultured and transfected as described in Prigge et al. (22). Photocurrents were determined using the whole-cell patch-clamp technique. Data was recorded with pClamp10.1 (Molecular Devices). A Polychrome V (TILL Photonics) was used as a light source that was controlled with TILLVISION software (TILL Photonics) and by a VS25 shutter (Vincent Associates UNIBLITZ). In contrast to oocyte action spectra measurements, light intensity was directly adjusted to an equal number of photons (1.35×10^{20} m^{-2}/s^{-1}) for all wavelengths using a software-controlled, motorized filter wheel (type NSND-3; Newport, San Diego, CA). The standard external solution contained: 140 mM NaCl, 2 mM $CaCl_2$, 2 $MgCl_2$, and 1 mM KCl with 10 HEPES (pH_o 7.2). The standard internal solution contained: 110 mM NaCl, 10 mM EGTA, 2 mM $MgCl_2$, 2 mM $CaCl_2$, 1 mM KCl, 1 mM CsCl, and 10 mM HEPES (pH_i 7.2).

Confocal microscopy

GR localization in HEK-293 cells was monitored 1 day after transfection by detecting enhanced cyan fluorescent protein (ECFP) fluorescence using a FluoView 1000 microscopy system (Olympus). Pictures were taken on a confocal LSM IX81 equipped with a 60× 1.2 Water UplanSApo objective (Olympus), and 440-nm LEDs were used to excite ECFP. Fluorescence emission was detected using a spectral photomultiplier-tube detector.

RESULTS

Characteristics of *Gloeobacter* rhodopsin wild-type

cRNA encoding the rhodopsin of *Gloeobacter violaceus* was injected into freshly prepared *Xenopus laevis* oocytes. After 4–5 days, photocurrents were measured upon 200-ms illumination at holding voltages between −125 mV and 50 mV (Fig. 1 *A*). The initial photocurrents decayed from an early maximum to a sustained stationary current under nearly all conditions; however, the peak current was more pronounced at alkaline pH_o. Positive currents revealed outward proton pumping. At day 5 after injection, stationary currents with amplitudes up to the 500 nA were recorded at the reference conditions (i.e., 0 mV, pH_o 7.5) and were dramatically larger than photocurrents recorded from BR and GPR with ~50–100 nA ((10,14) and see Fig. S1 *C* in the Supporting

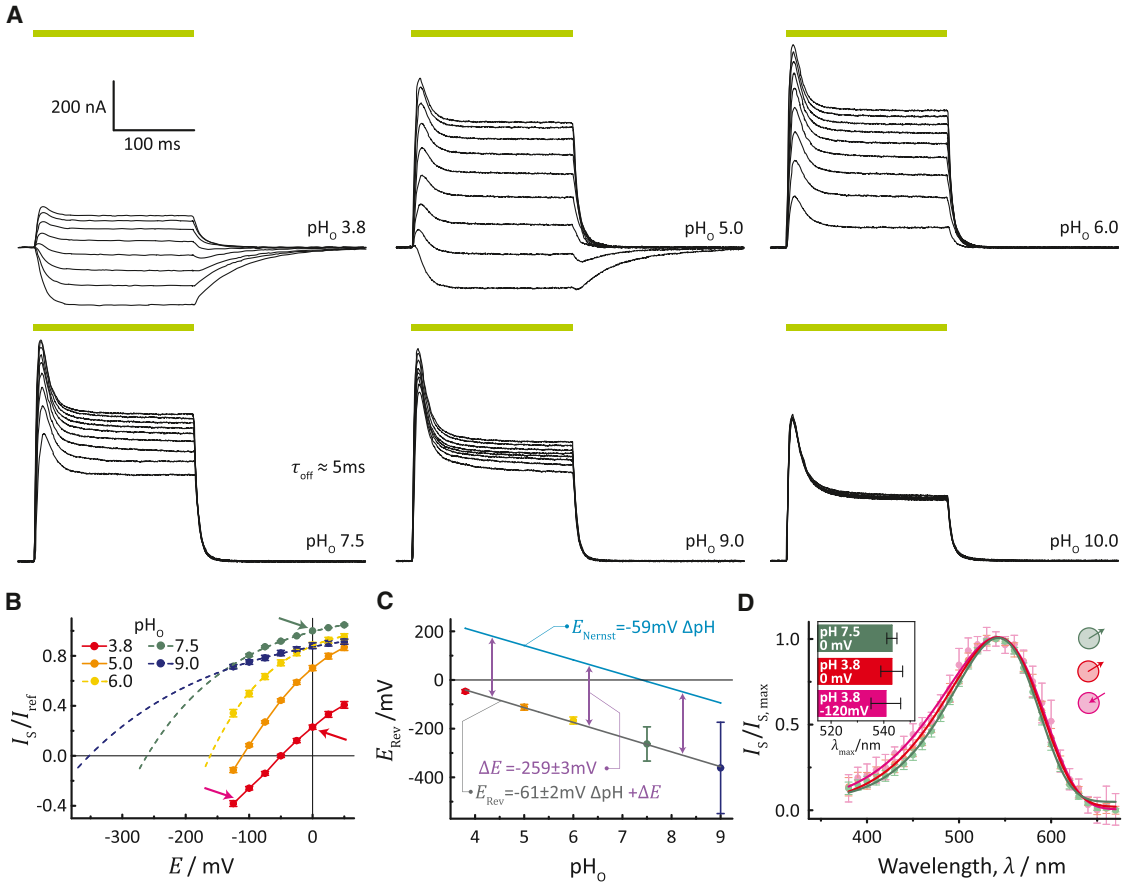

FIGURE 1 Basic characterization of GR-WT in *Xenopus laevis* oocytes. (*A*) Typical photocurrent traces of GR-WT at different extracellular pH conditions and holding voltages ranging from −125 mV up to +75 mV in 25-mV steps. A 200-ms pulse of green light (550 ± 25 nm) was used for activation of GR. (*B*) $I(E)$-plot of stationary currents with extrapolated reversal voltages (mean ± SE, $n \geq 13$). Currents were normalized to stationary photocurrent at pH$_o$ 7.5 and 0 mV (I_{ref}). (*Arrows*) Conditions for action spectra measurements. For pH$_o$ 6.0, 7.5, and 9.0 the reversal voltage was determined by nonlinear regression (*broken line*) according to $I(E) = I_0 + Ae^{bE}$. (*C*) Plot of the determined reversal voltages E_{rev} versus pH$_o$, fitted by linear regression. The reversal voltages calculated by the Nernst equation (E_{Nernst}) are based on an intracellular pH$_i$ of 7.4 (mean ± SD, $n \geq 13$). (*D*) Action spectra of stationary outward directed photocurrents at pH$_o$ 7.5 (*green*) and 3.8 (*red*) at 0 mV as well as for inward directed photocurrents at pH$_o$ 3.8 and −120 mV (*magenta*). Currents were normalized to the maximal stationary currents. (*Inset*) Action spectra maxima (mean ± SD, $n \geq 13$).

Material). Currents from GR showed significant voltage dependence between pH$_o$ 9 and 3.8, and were solely directed outward under all voltage conditions between pH$_o$ 6 and 10. At pH 10, the stationary currents were nearly voltage-independent. Interestingly, at pH$_o$ 5.0 and 3.8 the negative voltage stationary currents were inverted and directed inward. As the reversal voltage was approached, the outward-directed peak currents transited into stationary inward currents, as seen at −100 mV and pH$_o$ 5.0 (Fig. 1 *A*). This observation can be interpreted as an overlay of two transport modes, one directed outward and the other inward. As expected, the ratio of both depended on the electrochemical gradient.

The reversal voltages for pH values 6.0, 7.5, and 9.0 were determined by extrapolation (Fig. 1 *B*) and plotted together with the directly measured values for pH$_o$ 3.8 and 5.0 versus the membrane voltage (Fig. 1 *C*). All values were shifted by −260 mV relative to the Nernst potential, which was calculated with an assumed internal pH of 7.4 (23). The data suggest that the current became inverted whenever the load exceeded a maximum of −260 mV. The identical shifts of −260 mV for different pH$_o$ values demonstrate the equivalence of the chemical and electrical gradient respective electrochemical loads. Finally, all current amplitudes were independent of monovalent cations and anions in the medium, excluding any contributions of these ions to the pump current or inhibitory function, respectively (see Fig. S1). We observed a small reduction in current upon addition of 100 mM Mg^{2+} or Ca^{2+}, which was most likely due to a surface charge effect.

Next, we studied the wavelength dependence of the currents under variable conditions. The action spectra showed maxima near 540 nm with minor variations up to 4 nm for spectra recorded from pH$_o$ 9 to 3.8. Most interestingly, even the inward currents observed at pH 3.8 did not exhibit a spectral shift compared to pH 7.5 (Fig. 1 *D*). Because protonation of the RSB counterion is expected to cause spectral

shifts in practically all rhodopsins (24,25), we exclude a protonation change of the counterion complex as the mechanism behind the current inversion.

Modification of the RSB counterion complex

Because the protonation state of D121 remained unchanged after the switch from outward to inward currents, it could be hypothesized that the H^+-transfer function of the D121 carboxylic residue is dispensable. To test this, we substituted D121 with threonine. The mutant, GR-D121T, was nonfunctional and exhibited only small transient photocurrents (Fig. 2 *A*). These inward-directed transient currents were consistent with a proton release from the $RSBH^+$ toward the inner surface of the membrane. Moreover, this release was only visible at negative voltages (Fig. 2 *B*), thereby revealing that substantial H^+ movement—not pumping—occurred along the electrochemical gradient.

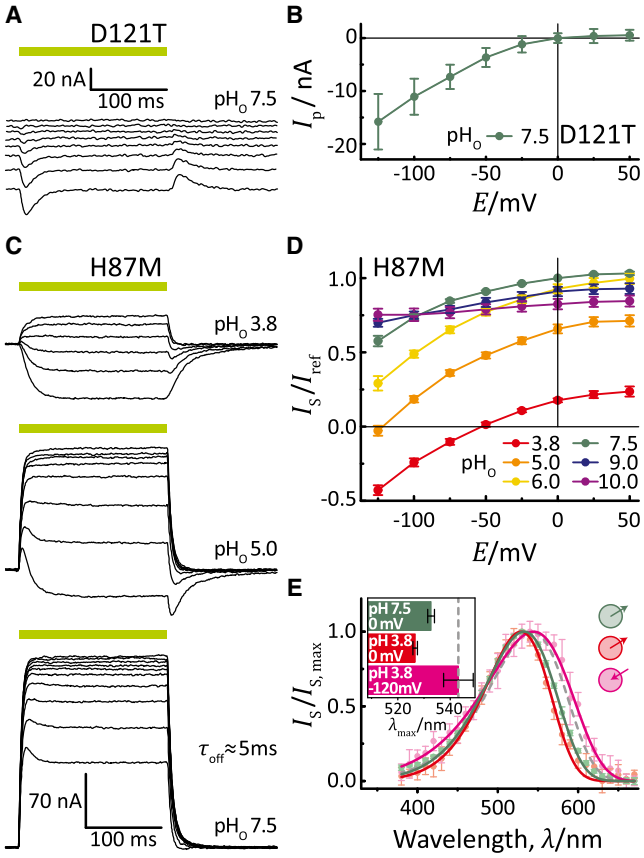

FIGURE 2 Detailed characterization of GR-D121T and GR-H87M in oocytes. (*A*) Representative GR-D121T-mediated transient inward-directed photocurrents measured at pH_o 7.5 and holding voltages between −125 mV and +75 mV in 25mV steps. (*B*) Resulting *I*(*E*)-Plot for GR-D121T (mean ± SE, $n = 7$). (*C*) Typical photocurrents of a GR-H87M expressing oocytes at different pH_o and membrane voltages from −125 mV up to +50 mV in 25-mV steps. (*D*) *I*(*E*)-plot for stationary currents of GR-H87M (mean ± SE, $n \geq 9$). (*E*) Action spectra for stationary currents of GR-H87M at different pH_o and voltages as measured for GR-WT (compare to Fig. 1 *D*). (*Inset*) Action spectra maxima (mean ± SD, $n \geq 6$).

Thus, in the absence of a negative counterion, the $RSBH^+$ proton was released to the internal side of the protein during the photocycle. The extent of the charge displacement depended on the membrane voltage. However, for both active outward pumping and sustained passive inward currents, the H^+ transfer function of D121 was required.

GPR shows a strong pH dependence on the absorption spectrum in detergent caused by the high pK_a of D97, which functions as the primary acceptor of the RSB proton (26). The high $pK_a = 7.1$ is a result of the hydrogen-bridged contact of D97 to the nearby H75. Because this histidine is conserved within the PR evolutionary clade, a high pK_a for the Schiff base counterion is considered a general property of all PRs and related pumps (27–29). However, a previous study reported that the *Exiguobacterium sibiricum* (ESR) proton pump, which also contains the corresponding histidine, exhibits a low counterion pK_a and marginal spectral pH dependence between pH 3 and 9 (30). Mutation of this histidine (H57) to methionine shifted the pK_a of the counterion to higher values (as observed for Green PR) and caused protonation of the counterion at relatively moderate acidic conditions (pH_o) (30). Consistent with the pH-insensitivity of the GR spectrum, the influence of the homologous H87 on the Schiff counterion pK_a in GR may be similar to ESR yet substantially different from Green PR.

To assess the role of H87 on the RSB counterion in GR, we replaced H87 with alanine or methionine. Both GR-H87A and GR-H87M were still active pumps and showed inward-directed currents at low pH. With respect to current traces and *I*(*E*)-relations, GR-H87M was quite similar to *Gloeobacter* rhodopsin wild-type (GR-WT), even though the current amplitudes were smaller and the peak currents were less developed (Fig. 2, *C* and *D*). The kinetics were slightly faster, as observed previously for the analogous mutation in GPR (see Fig. S5 *C*) (28). The spectral maximum of GR-H87M was blue-shifted by 10 nm at neutral pH (λ_{max} at 533nm) relative to GR-WT. However, the H87M spectrum of the inward currents recorded at high load with −120 mV and pH_o 3.8 was shifted bathochromic by 16 nm compared to 0 mV, suggesting that in this case the D121 counterion was protonated at low pH_o during the dark state (Fig. 2 *E*), similar to the homologous ESR mutant. This experiment supports the notion that the protonation state of the counterion complex is irrelevant for the observed inward currents. GR-H87A did not show any spectral shift at low pH_o due to lack of interaction between alanine and D121 (see Fig. S2).

Because it was conceivable that our inability to protonate D121 in oocytes may be caused by only unilateral acidification, we transiently expressed GR-WT and GR-H87M in HEK-293 cells and measured the whole-cell photocurrent. Although only a small fraction was integrated into the membrane as shown for WT, in Fig. 3 *A* the expression was sufficient for representative measurements (Fig. 3 *B*). Photocurrents were similar to oocyte experiments with low

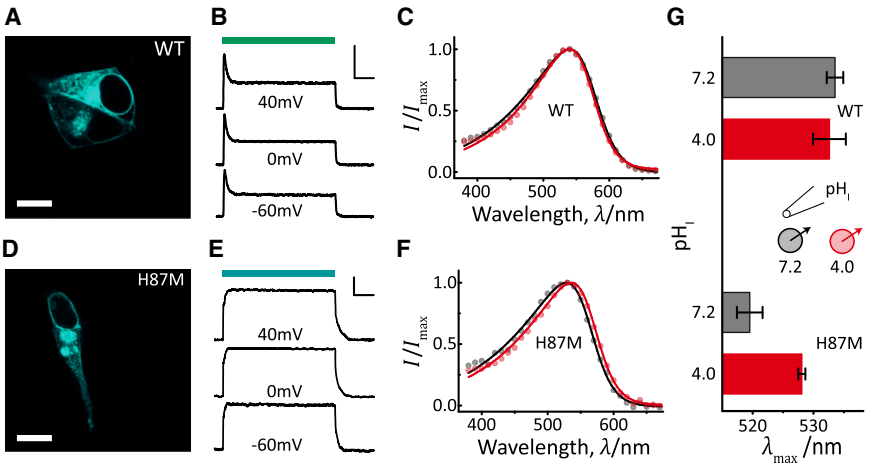

FIGURE 3 Characterization of GR-WT and GR-H87M expressed in HEK cells. (*A* and *D*) Confocal images of transfected HEK-293 cells. ECFP was monitored one day after transfection. Scale bar: 10 μm. (*B*) Typical photocurrents of GR-WT are shown. Photo activation was achieved with light of 540 $\pm$ 7 nm (scale bar: 100 pA and 50 ms). (*C* and *F*) Action spectra for GR-WT peak currents (*C*) and GR-H87M stationary currents (*F*) measured at intracellular pH_i 7.2 (*black*) and 4.0 (*red*), while pH_o was kept at 7.2 and 0 mV membrane potential. Only mean values are shown to visualize spectral shifts. Note that deviations were similar spectral measurements in oocytes (GR-WT, $n \geq 8$; GR-H87M, $n = 5$). (*E*) Typical photocurrents of GR-H87M. Photo activation was achieved with light of 520 $\pm$ 7 nm (scale bar: 100 pA and 50 ms). (*G*) Comparison of action spectra maxima from panels *C* and *F* (mean $\pm$ SD, $n \geq 5$).

voltage dependence for both peak and stationary currents at neutral pH (see Fig. S4 *B*). HEK cell experiments provided the complementary information that low internal pH_i keeps the WT spectrum almost unchanged (Fig. 3, *C* and *G*) and current inversion was prevented, as expected.

For H87M, membrane targeting was again poor (Fig. 3 *D*) and the transient currents were again completely missing (Fig. 3 *E*). The spectrum of H87M is blue-shifted by 14 nm relative to wild-type and shifted back almost to the wild-type peak after internal acidification (Fig. 3, *F* and *G*). The acid-shift was likely due to small extracellular pH changes because the shift was less pronounced compared to external acidification. These experiments reveal that internal pH has a minor influence on the resulting spectrum and—as expected—reduced the electrochemical load.

Mutation of E132 and S77

Another characteristic of all proteorhodopsins and related pumps is that a glutamate residue reprotonates the RSB during the photocycle. In contrast, an aspartate residue carries out this role in most archaeal pumps, such as D96 in BR (31–33). Substitution of E132 with aspartate in GR kept the photocurrents at neutral pH nearly unchanged (Fig. 4 *A*). Interestingly, the voltage dependence of the currents was stronger compared to WT (see traces at pH 7.5). At negative voltage and acidic conditions, the current amplitudes were reduced drastically but sign inversion did only barely occur (Fig. 4, *A* and *C*). The lack of inward currents in the mutant may be due to aggravated deprotonation because of a lower pK_a, which may be caused by stabilized bridging of the protonated aspartate to adjacent H^+-acceptors (34).

To better understand this phenomenon, we examined the three-dimensional structure of Xanthorhodopsin (XR), which is related to GR (29). In XR, the homologous E107 is H^+-bridged to water (Wat-502) and only indirectly associated with S52 (analogous to S77 in GR). In BR, however, the homologous D96 is directly bridged to T46. This hydrogen bridge becomes dissociated during the photocycle upon formation of the N-state when the H^+ is transferred to

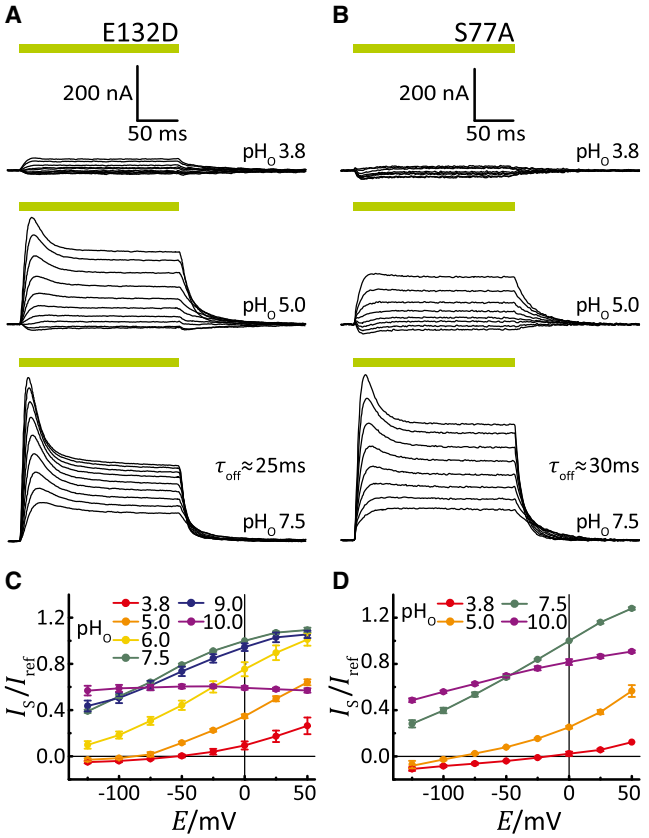

FIGURE 4 (*A* and *B*) Photocurrents of GR-E132D (*A*) and GR-S77A (*B*) at different extracellular pH_o conditions and holding voltages between -125 mV and $+75$ mV in 25-mV steps. (*C* and *D*) *I*(*E*) plots of stationary currents of GR-E132D (*C*) and GR-S77A (*D*) versus the holding potential at different pH_o values (mean $\pm$ SE, $n \geq 9$ (E132D), $n = 4$ (S77A)).

the RSB (35). To test the relevance of the E132-S77 connection in GR, we replaced S77 with alanine or cysteine. Both mutants, GR-S77A and GR-S77C, were active and exhibited similar characteristics to GR-E132D, with only evanescent currents observed at low pH (Fig. 4, *B* and *D*, and see Fig. S3). Based on these data, we conclude that mutation of either E132 or S77 modifies hydrogen bridging between these residues with a concomitant decline in the pK_a of the E132 H^+-donor.

Kinetic properties of GR-WT and E132D

Because previous studies demonstrated that inward-directed currents are prevented in BR and AR and both pumps possess an aspartate at the position homologous to GR-E132, the Glu/Asp substitution may be considered an advantage. Interestingly, our data demonstrate that the kinetics of GR-E132D was slower compared to GR-WT (Fig. 5, *A–D*). Consequently, the photocurrent of the mutant became saturated at lower light intensities. Outward-directed currents of GR-WT were characterized by fast, quite voltage-independent τ_{off} values of ~5–7 ms at pH_o 5 to 10 with only slight increase under acidic conditions (Fig. 5 *A* and see Fig. S5). In contrast, τ_{off} of GR-E132D was both more voltage- and pH_o-dependent (Fig. 5, *C* and *D*, and see Fig. S5), ranging from 50 ms at pH 5 (−25 mV) to 5 ms at pH 7.5 (50 mV).

Accumulation of late photocycle intermediates at high light intensities results in decreased current amplitudes and the appearance of the transient fraction of the current. The decay of late photocycle intermediates in darkness correlates with recovery of the transient fraction, as seen from experiments with double light pulses of different delay (Fig. 5 *E*). This recovery was also slower in E132D (τ_{rec} = 76 ms) compared to WT (τ_{rec} = 50 ms) (Fig. 5 *F*). Most clearly, a comparison of the WT and mutant amplitudes demonstrated that WT is more efficient than both H87M and E132D (Fig. 5 *G*).

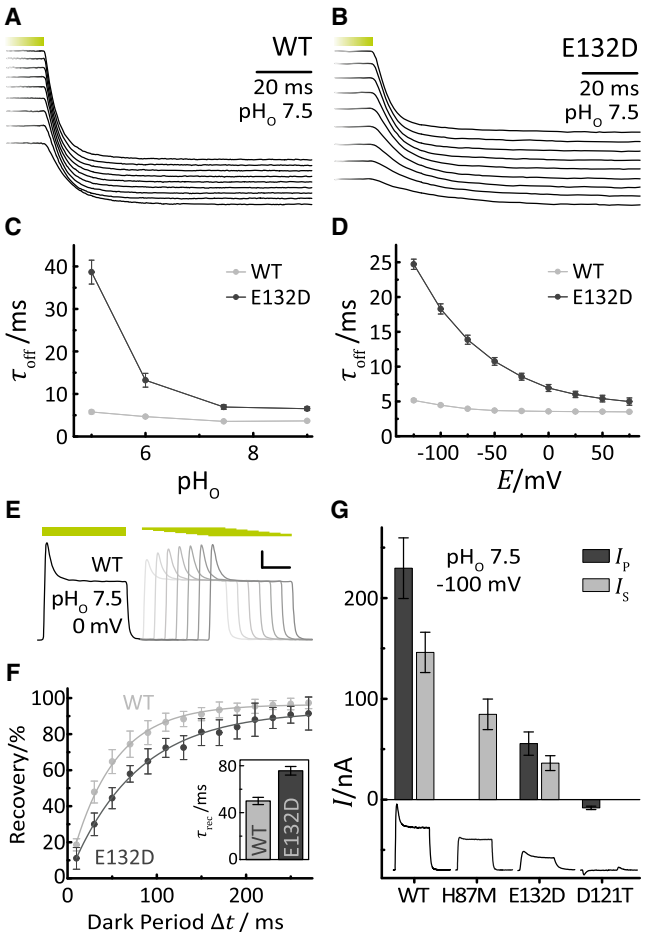

FIGURE 5 Kinetic properties and photocurrent amplitudes of GR-WT and GR-E132D. (*A* and *B*) Current trace cuts of GR-WT (*A*) and GR-E132D (*B*) expressing oocytes at pH_o 7.5 and holding voltages between −125 mV and +75 mV in 25-mV steps (*bottom* to *top*). (*C* and *D*) Characteristics of τ_{off} for GR-WT (*C*) and GR-E132D (*D*) at different pH_o values and holding voltages (mean ± SE, $n \geq 9$ (WT), $n \geq 6$ (E132D)). (*E*) Representative double pulse experiment of GR-WT at pH_o 7.5 and 0 mV. During repetitive experiments the dark interval between the two light pulses was gradually expanded to determine the recovery of the transient while the stationary current remained unchanged. The intersweep dark period was always 16 s to guarantee completed dark adaption. (*F*) Plot of the second transient versus time for GR-WT and GR-E132D at pH_o 7.5 and 0 mV. (*Inset*) Resulting τ_{rec} values (mean ± SE, $n \geq 6$). (*G*) Comparison of peak and stationary photocurrent amplitudes. Photocurrents of E132D are compared with WT and other mutants for pH_o 7.5 and −100 mV. The peak current amplitudes of GR-WT amount to 630 nA for comparison (mean ± SE, $n \geq 7$).

DISCUSSION

Results from the presented experiments show that the *Gloeobacter* rhodopsin GR is an active proton pump with a maximal pumping load of ~−260 mV over a broad pH range. Extrapolated reversal voltages from earlier studies suggest that the maximal forces of the BR, GPR, and AR ion pumps are quite similar and are all in this range (3,9,11,14). However, the current generated by BR, AR, and GR-E132D did not invert at low pH_o, and instead approaches zero at loads near −260 mV or beyond (Fig. 4 *C* in this work, and see Fig. 2 *C* in Geibel et al. (11) and Fig. 2 *D* in Tsunoda et al. (3)) whereas GPR and GR currents invert at high electrochemical load.

Because the inward currents observed for GPR at high load were all directed along an electrochemical gradient, these currents are of purely passive nature and are promoted by the high pK_a of E108. However, in GPR, the pK_a could not be upshifted by the E108D mutant and GPR remained leaky (14,15), suggesting that the details surrounding the hydrogen-bonding network are different in the two proteins.

We developed a Xanthorhodopsin-based GR model that explains both active transport against a gradient and passive proton translocation along a gradient and we compared this model with three-dimensional structures of BR. The crystal structure of the BR dark-state (36) is characterized by direct

contact between D96 and T46, suggesting hydrogen bridging between these two residues and two decisive water molecules in the inner half-channel (Wat-501, Wat-502). However, Fourier-transform infrared spectroscopy studies identified a third highly mobile water molecule named Wat-501b. This water has been seen in the structure of the photocycle intermediate M1 (PDB:1P8H) even before the pronounced helix movement occurs upon approaching the late M2 state. These three water molecules are rearranged during the late M to N transition by protein conformation changes to form the necessary Grotthuss proton wire between Asp^{96} and the Schiff-base nitrogen before the proton is transferred accordingly (37) (Fig. 6 *A*). In contrast, typical for XR is the proton donor E107, which is connected to the S52 via a water molecule that also connects E107 with the retinal-binding K240, which is in closer proximity compared to BR (Fig. 6 in Luecke et al. (29)). In GR this structural feature is expected to be conserved (Fig. 6 *B*), and the hydrogen-bridged water among GR-E132, GR-S77, and the backbone of GR-K257 has been experimentally identified by vibrational spectroscopy (38). The presence of this water molecule in the cytoplasmic cavity between RSB and the inner surface renders the GR dark state similar to the known BR-early-N structure (35) (Fig. 6 *C*). Water rearrangement with concomitant separation of BR-D96 and T46, and decline in D96-pK_a, is needed for the proton transfer to the RSB and completion of the cycle (37,40).

Fig. 6 *D* illustrates the potential H^+-transfer in GR based on the model presented in Fig. 6 *B*. For simplicity, only one water molecule is depicted near the RSBH (in BR Wat-402). However, Fourier-transform infrared spectroscopy suggests that the three-dimensional counterion complex actually consists of GR-D121, GR-D253, and three water molecules similar to BR (21). As mentioned above, GR-D121 acts as the proton transfer residue for both inward- and outward-directed currents and its pK_a is below 3.8, which means it is not protonated up to a bulk pH_o of 3.8. Because H87 does not function as a pK_a modifier in GR, this residue is not shown in the model. The cytoplasmic side of GR-E132 is protonated similar to BR-D96 in darkness at neutral pH; however, deprotonation occurs during the M to N transition as in case of BR (41). At low pH and negative membrane voltage, the situation in GR changes (Fig. 6 *E*). We predict that under these conditions GR-E132 is already deprotonated in the dark state and deprotonation is facilitated by hydrogen bonding to water. The hydrogen-bonding network on the intracellular portion of the protein connects GR-E132 to the protonated Schiff base. After retinal

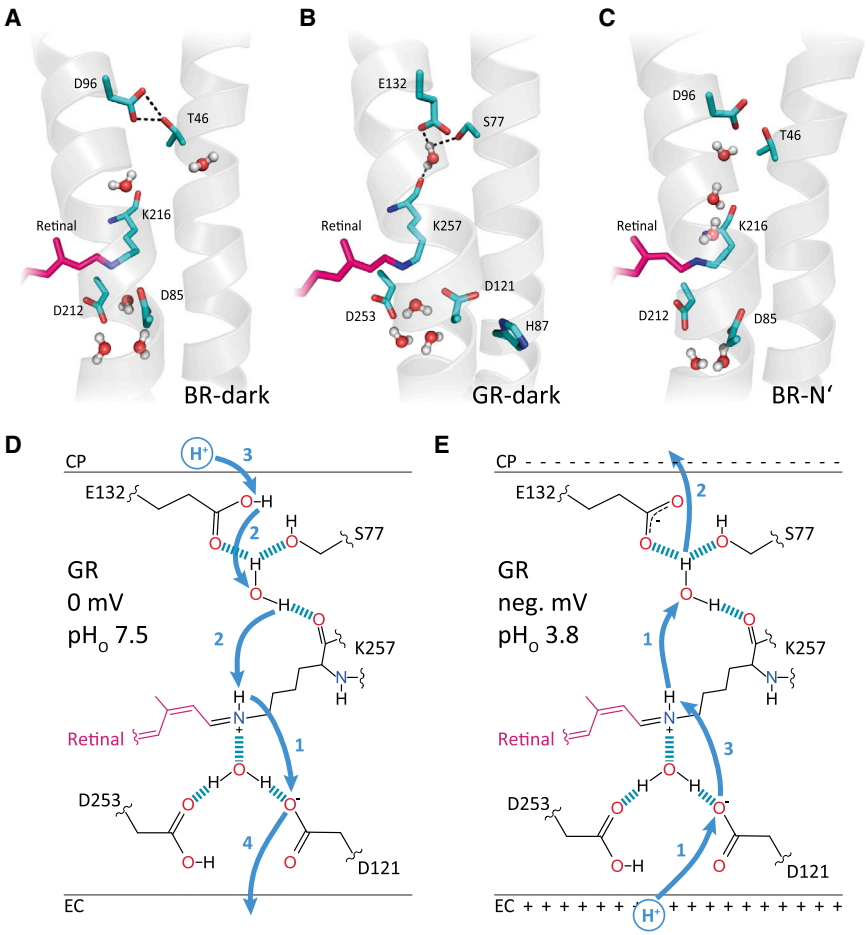

FIGURE 6 Scheme of the proposed model for different transport modes mediated by GR-WT. (*A*) Structure section of BR-WT dark state (PDB:1M0L, 1.47 Å). Water molecules at the cytoplasmic side are shown according to Freier et al. (37). (*B*) Model of the predicted dark state structure of GR-WT based on the known Xanthorhodopsin structure (PDB:3DDL, 1.90 Å) for standard conditions (pH_o 7.5, 0 mV). The water cluster near D121, D253, and the protonated Schiff base is assumed to be similar to BR. Between E132 and S77, at least one water molecule is inserted that is also in close distance to the backbone of K257. (*C*) Structural section of BR-WT during the late photocycle N-intermediate (PDB:1P8U, 1.62 Å). The late N-intermediate is characterized by reprotonation of the RSB from the primary proton donor D96 via a water chain. Full assembly of the water chain between D96 and the Schiff base is developed during the M to N transition. Protein hydrogens are not shown. (*D* and *E*) Model of proton translocation in GR-WT show as dark-state model without (*D*) and with (*E*) applied negative electrochemical gradients. (*Arrows*) Assumed proton movements.

isomerization and switching of the H^+ to the internal side of the Schiff base, the pK_a of the Schiff base dramatically decreases (42) and the H^+ is now released to the intracellular bulk phase via E132.

This inward-directed H^+ release is prevented in BR for two main reasons: lack of long-range interaction between the RSB and BR-D96 during the early reactions of the photocycle, and the higher pK_a of BR-D96. Thus, we propose that replacement of E132 with aspartate in GR increases the pK_a of this residue toward that of BR due to loss of hydrogen bonding.

The argument of Friedrich et al. (14) and Lörinczi et al. (15) is quite different and not in line with our model, although their measurements on GPR are similar to the results we presented above for GR and to our understanding fully compatible with our model. The authors argue that at acidic conditions in wild-type GPR the RSB counterion Asp^{97} (corresponding to GR-D121 and BR-D85) is protonated in the dark, thereby promoting H^+ release from the RSB toward the intracellular site of the membrane. This argument results from spectroscopic studies on GPR in detergent where D97 protonates at relatively mild acidic conditions (pK_a between 7.1 and 7.7 (14,26)). However, deprotonation has not been substantiated for GPR in oocytes by action spectroscopy. Even more important is the fact that inward-directed currents are observed only when at low pH_o an additional membrane voltage is applied (14,15). Moreover, we have demonstrated for GR that for inward-directed passive proton translocation, the protonation state of the chromophore counterion is irrelevant, although only chromophores with deprotonated counterion are able to pump protons actively. Therefore, in the light of our data on GR, it is likely that inward-directed currents mediated by GPR are not determined by protonation of D97 but instead, like in GR, caused by the low pK_a of GPR-E108, the residue responsible for RSB reprotonation at small load. In line with this argument is the observation of Lakatos et al. (18) and Váró et al. (19) on purified GPR preoriented in acrylamide gels: charge displacement is blocked at low pH when the counterion D97 is protonated, supporting that active pumping requires a deprotonated counterion, whereas passive inward-directed proton translocation does not.

Biological function of GR and Glu^{132}

In principle, it is clear that GR could support ATP synthesis at physiological conditions in *Gloeobacter violaceus* due to the lack of functional thylakoids and low levels of chlorophyll-dependent photosynthesis (43). Furthermore, published reports have demonstrated that *Gloeobacter violaceus* has a low capacity for intracellular pH homeostasis (44). Thus, it would not be surprising if GR is involved in these processes. A different but complementary explanation would be that the function of GR could be to sustain a provisional membrane voltage under conditions where chlorophyll-based photosynthesis is depleted. Recently, Marchetti et al. (45) reported a meta-transcriptomic analysis of iron-limited eukaryotic plankton (mostly diatoms). They identified rhodopsin sequences in the oceanic diatoms *Pseudo-nitzschia granii* and *Fragilariopsis cylindrus* and the haptophyte *Phaeocystis globosa*. The rhodopsin transcripts were upregulated in libraries isolated during low iron supply. This conclusion is supported by Raven (46), which suggested that the high iron requirements in oxygenic photosynthesis and lack of trace metal requests rendered rhodopsins advantageous over oxygenic photosynthesis at low-iron environments.

Comparison of proteorhodopsins from marine algae to those of terrestrial cyanobacteria suggests that these light-driven ion pumps are active whenever chlorophyll-dependent photosynthesis is low. For this supportive role, the pumps have been optimized during evolution with respect to speed and not respective activity over a maximal pH range.

SUPPORTING MATERIAL

Five figures are available at http://www.biophysj.org/biophysj/supplemental/S0006-3495(13)00978-8.

We thank Maila Reh for preparing oocytes and Sergei P. Balashov and Janos K. Lanyi (University of California, Irvine) for providing expression plasmids encoding GR-WT and GR-H87M and for thoughtful discussion. We also thank Thomas Korte and Andreas Herrmann (Humboldt-Universität zu Berlin) for help with fluorescence microscopy.

The work was supported by the Leibniz Graduate School of Molecular Biophysics (to A.V.) and the Deutsche Forschungsgemeinschaft (DFGgrant Nos. HE3824/9-4 and B2-SFB-1078 to P.H.).

REFERENCES

1. Béjà, O., L. Aravind, …, E. F. DeLong. 2000. Bacterial rhodopsin: evidence for a new type of phototrophy in the sea. *Science.* 289:1902–1906.

2. Waschuk, S. A., A. G. Bezerra, Jr., …, L. S. Brown. 2005. *Leptosphaeria* rhodopsin: bacteriorhodopsin-like proton pump from a eukaryote. *Proc. Natl. Acad. Sci. USA.* 102:6879–6883.

3. Tsunoda, S. P., D. Ewers, …, P. Hegemann. 2006. H^+-pumping rhodopsin from the marine alga *Acetabularia*. *Biophys. J.* 91:1471–1479.

4. Lanyi, J. K. 2006. Proton transfers in the bacteriorhodopsin photocycle. *Biochim. Biophys. Acta.* 1757:1012–1018.

5. Stoeckenius, W., R. H. Lozier, and W. Niederberger. 1977. Photoreactions of bacteriorhodopsin. *Biophys. Struct. Mech.* 3:65–68.

6. Herrmann, T. R., and G. W. Rayfield. 1976. A measurement of the proton pump current generated by bacteriorhodopsin in black lipid membranes. *Biochim. Biophys. Acta.* 443:623–628.

7. Bamberg, E. 1977. Rhodopsin and other proteins in artificial lipid membranes. *Biophys. Struct. Mech.* 3:39–42.

8. Braun, D., N. A. Dencher, …, M. P. Heyn. 1988. Nonlinear voltage dependence of the light-driven proton pump current of bacteriorhodopsin. *Biophys. J.* 53:617–621.

9. Drachev, L. A., A. A. Jasaitis, …, V. P. Skulachev. 1974. Direct measurement of electric current generation by cytochrome oxidase, H^+-ATPase and bacteriorhodopsin. *Nature.* 249:321–324.
10. Nagel, G., B. Möckel, …, E. Bamberg. 1995. Functional expression of bacteriorhodopsin in oocytes allows direct measurement of voltage dependence of light induced H^+ pumping. *FEBS Lett.* 377:263–266.
11. Geibel, S., T. Friedrich, …, E. Bamberg. 2001. The voltage-dependent proton pumping in bacteriorhodopsin is characterized by optoelectric behavior. *Biophys. J.* 81:2059–2068.
12. Michel, H., and D. Oesterhelt. 1976. Light-induced changes of the pH gradient and the membrane potential in *H. halobium*. *FEBS Lett.* 65:175–178.
13. Váró, G., and J. K. Lanyi. 1989. Photoreactions of bacteriorhodopsin at acid pH. *Biophys. J.* 56:1143–1151.
14. Friedrich, T., S. Geibel, …, E. Bamberg. 2002. Proteorhodopsin is a light-driven proton pump with variable vectoriality. *J. Mol. Biol.* 321:821–838.
15. Lörinczi, E., M. K. Verhoefen, …, T. Friedrich. 2009. Voltage- and pH-dependent changes in vectoriality of photocurrents mediated by wild-type and mutant proteorhodopsins upon expression in *Xenopus* oocytes. *J. Mol. Biol.* 393:320–341.
16. Wang, W. W., O. A. Sineshchekov, …, J. L. Spudich. 2003. Spectroscopic and photochemical characterization of a deep ocean proteorhodopsin. *J. Biol. Chem.* 278:33985–33991.
17. Dioumaev, A. K., J. M. Wang, …, J. K. Lanyi. 2003. Proton transport by proteorhodopsin requires that the retinal Schiff base counterion Asp-97 be anionic. *Biochemistry.* 42:6582–6587.
18. Lakatos, M., J. K. Lanyi, …, G. Váró. 2003. The photochemical reaction cycle of proteorhodopsin at low pH. *Biophys. J.* 84:3252–3256.
19. Váró, G., L. S. Brown, …, J. K. Lanyi. 2003. Characterization of the photochemical reaction cycle of proteorhodopsin. *Biophys. J.* 84:1202–1207.
20. Nakamura, Y., T. Kaneko, …, S. Tabata. 2003. Complete genome structure of *Gloeobacter violaceus* PCC 7421, a cyanobacterium that lacks thylakoids. *DNA Res.* 10:137–145.
21. Hashimoto, K., A. R. Choi, …, H. Kandori. 2010. Low-temperature FTIR study of *Gloeobacter* rhodopsin: presence of strongly hydrogen-bonded water and long-range structural protein perturbation upon retinal photoisomerization. *Biochemistry.* 49:3343–3350.
22. Prigge, M., F. Schneider, …, P. Hegemann. 2012. Color-tuned channelrhodopsins for multiwavelength optogenetics. *J. Biol. Chem.* 287:31804–31812.
23. Cicirelli, M. F., K. R. Robinson, and L. D. Smith. 1983. Internal pH of *Xenopus* oocytes: a study of the mechanism and role of pH changes during meiotic maturation. *Dev. Biol.* 100:133–146.
24. Wanko, M., M. Hoffmann, …, M. Elstner. 2008. Effect of polarization on the opsin shift in rhodopsins. 1. A combined QM/QM/MM model for bacteriorhodopsin and pharaonis sensory rhodopsin II. *J. Phys. Chem. B.* 112:11462–11467.
25. Altun, A., S. Yokoyama, and K. Morokuma. 2008. Quantum mechanical/molecular mechanical studies on spectral tuning mechanisms of visual pigments and other photoactive proteins. *Photochem. Photobiol.* 84:845–854.
26. Dioumaev, A. K., L. S. Brown, …, J. K. Lanyi. 2002. Proton transfers in the photochemical reaction cycle of proteorhodopsin. *Biochemistry.* 41:5348–5358.
27. Bergo, V. B., O. A. Sineshchekov, …, J. L. Spudich. 2009. His-75 in proteorhodopsin, a novel component in light-driven proton translocation by primary pumps. *J. Biol. Chem.* 284:2836–2843.
28. Hempelmann, F., S. Hölper, …, C. Glaubitz. 2011. His^{75}-Asp^{97} cluster in green proteorhodopsin. *J. Am. Chem. Soc.* 133:4645–4654.
29. Luecke, H., B. Schobert, …, J. K. Lanyi. 2008. Crystallographic structure of xanthorhodopsin, the light-driven proton pump with a dual chromophore. *Proc. Natl. Acad. Sci. USA.* 105:16561–16565.
30. Balashov, S. P., L. E. Petrovskaya, …, J. K. Lanyi. 2012. Aspartate-histidine interaction in the retinal Schiff base counterion of the light-driven proton pump of *Exiguobacterium sibiricum*. *Biochemistry.* 51:5748–5762.
31. Man, D., W. Wang, …, O. Béjà. 2003. Diversification and spectral tuning in marine proteorhodopsins. *EMBO J.* 22:1725–1731.
32. Petrovskaya, L. E., E. P. Lukashev, …, M. P. Kirpichnikov. 2010. Predicted bacteriorhodopsin from *Exiguobacterium sibiricum* is a functional proton pump. *FEBS Lett.* 584:4193–4196.
33. Rothschild, K. J., T. Marti, …, H. G. Khorana. 1993. Asp^{96} deprotonation and transmembrane α-helical structural changes in bacteriorhodopsin. *J. Biol. Chem.* 268:27046–27052.
34. Pace, C. N., G. R. Grimsley, and J. M. Scholtz. 2009. Protein ionizable groups: pK values and their contribution to protein stability and solubility. *J. Biol. Chem.* 284:13285–13289.
35. Schobert, B., L. S. Brown, and J. K. Lanyi. 2003. Crystallographic structures of the M and N intermediates of bacteriorhodopsin: assembly of a hydrogen-bonded chain of water molecules between Asp-96 and the retinal Schiff base. *J. Mol. Biol.* 330:553–570.
36. Schobert, B., J. Cupp-Vickery, …, J. Lanyi. 2002. Crystallographic structure of the K intermediate of bacteriorhodopsin: conservation of free energy after photoisomerization of the retinal. *J. Mol. Biol.* 321:715–726.
37. Freier, E., S. Wolf, and K. Gerwert. 2011. Proton transfer via a transient linear water-molecule chain in a membrane protein. *Proc. Natl. Acad. Sci. USA.* 108:11435–11439.
38. Miranda, M. R., A. R. Choi, …, L. S. Brown. 2009. The photocycle and proton translocation pathway in a cyanobacterial ion-pumping rhodopsin. *Biophys. J.* 96:1471–1481.
39. Reference deleted in proof.
40. Kamikubo, H., M. Kataoka, …, J. K. Lanyi. 1996. Structure of the N intermediate of bacteriorhodopsin revealed by x-ray diffraction. *Proc. Natl. Acad. Sci. USA.* 93:1386–1390.
41. Gerwert, K., B. Hess, …, D. Oesterhelt. 1989. Role of aspartate-96 in proton translocation by bacteriorhodopsin. *Proc. Natl. Acad. Sci. USA.* 86:4943–4947.
42. Braiman, M. S., A. K. Dioumaev, and J. R. Lewis. 1996. A large photolysis-induced pKa increase of the chromophore counterion in bacteriorhodopsin: implications for ion transport mechanisms of retinal proteins. *Biophys. J.* 70:939–947.
43. Rippka, R., J. Waterbury, and G. Cohenbazire. 1974. Cyanobacterium, which lacks thylakoids. *Arch. Microbiol.* 100:419–436.
44. Belkin, S., R. J. Mehlhorn, and L. Packer. 1987. Proton gradients in intact cyanobacteria. *Plant Physiol.* 84:25–30.
45. Marchetti, A., D. M. Schruth, …, E. V. Armbrust. 2012. Comparative metatranscriptomics identifies molecular bases for the physiological responses of phytoplankton to varying iron availability. *Proc. Natl. Acad. Sci. USA.* 109:E317–E325.
46. Raven, J. A. 2009. Functional evolution of photochemical energy transformations in oxygen-producing organisms. *Funct. Plant Biol.* 36:505–515.

SUPPORTING MATERIAL

for

"Gloeobacter Rhodopsin, Limitation of Proton Pumping at High Electrochemical Load"

Arend Vogt, Jonas Wietek, and Peter Hegemann

From Institute of Biology, Experimental Biophysics, Humboldt-Universität zu Berlin, Invalidenstraße 42, 10115 Berlin, Germany

*Correspondence: hegemape@rz.hu-berlin.de

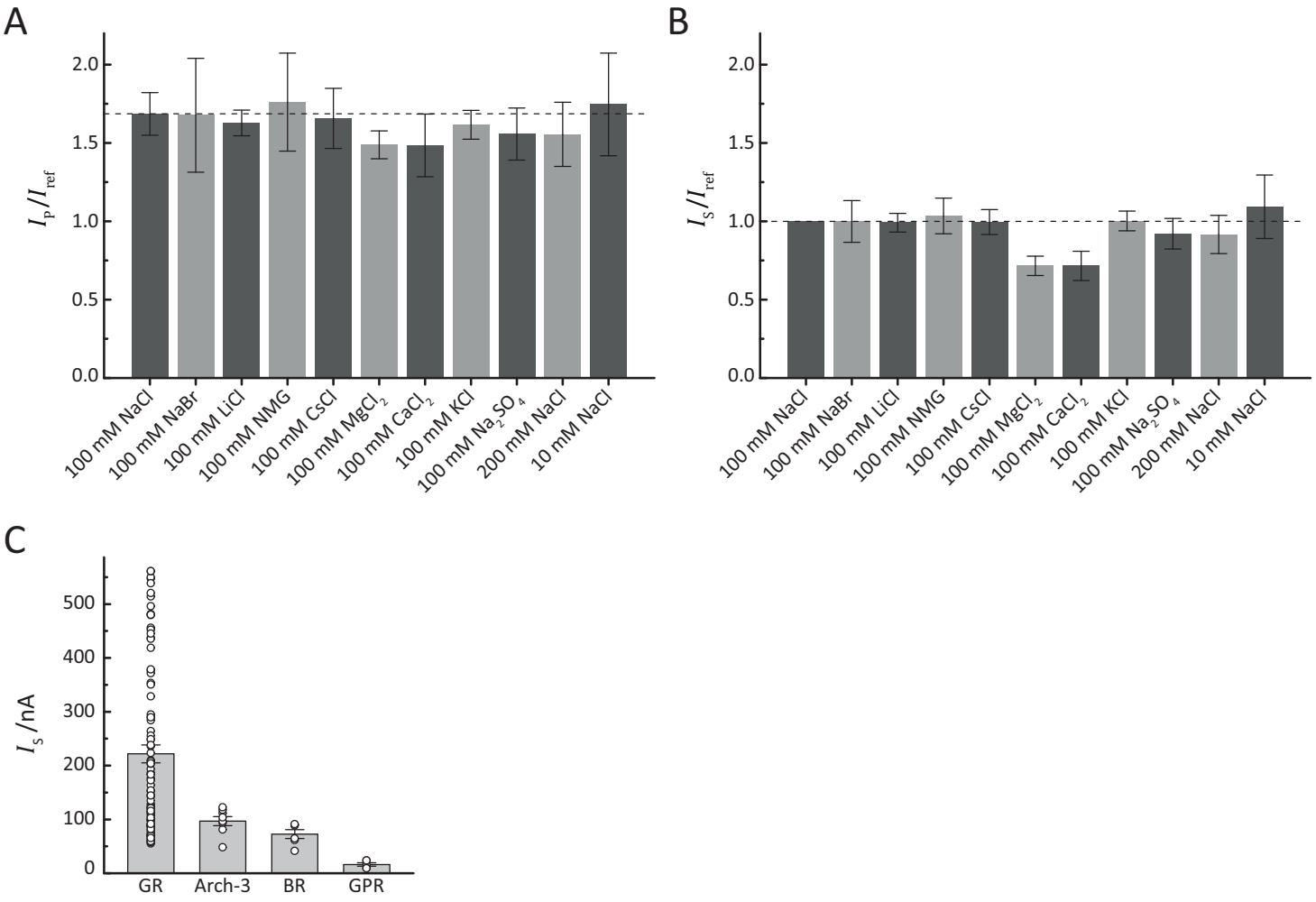

Figure S1. Ion selectivity and absolute photocurrent amplitudes of Gloeobacter Rhodopsin. Oocytes expressing GR-WT were activated by green light of 550±25 nm and photocurrents were recorded at a holding voltage of 0 mV. Different extracellular buffers were tested to test ion selectivity. No crucial differences were observable for peak currents (A) as well as stationary currents (B). Small current reduction in case of high concentrations of divalent cations can be explained by a surface charge effects. The results confirm that GR transports only protons. The extracellular buffer contained the following additional components [mM]: 1 $MgCl_2$, 0.1 $CaCl_2$ and 5 MOPS (pH_o 7.5, adjusted with NMG) (mean ± SD, n ≥ 8). C. Comparison of stationary photocurrent amplitudes (mean ± SE) of different proton pumping rhodopsins. Open dots indicate single measurement values. All proton pumps were expressed and measured under the same conditions (pH_o 7.5, 0 mV and 550±25 nm). Only GPR was excited with twofold increased light intensity (400-600 nm filter) due to low photocurrent amplitudes. This comparison underlines the high photocurrents of GR compared to GPR. GR: Gloeobacter Rhodopsin from *Gloeobacter violaceus* (n=89), Arch-3: Archaerhodopsin-3 from *Halorubrum sodomense* (n=8), BR: Bacteriorhodopsin from *Halobacterium salinarum* (n=6), GPR: Green Proteorhodopsin from γ-proteobacterium EBAC31A08 (n=5).

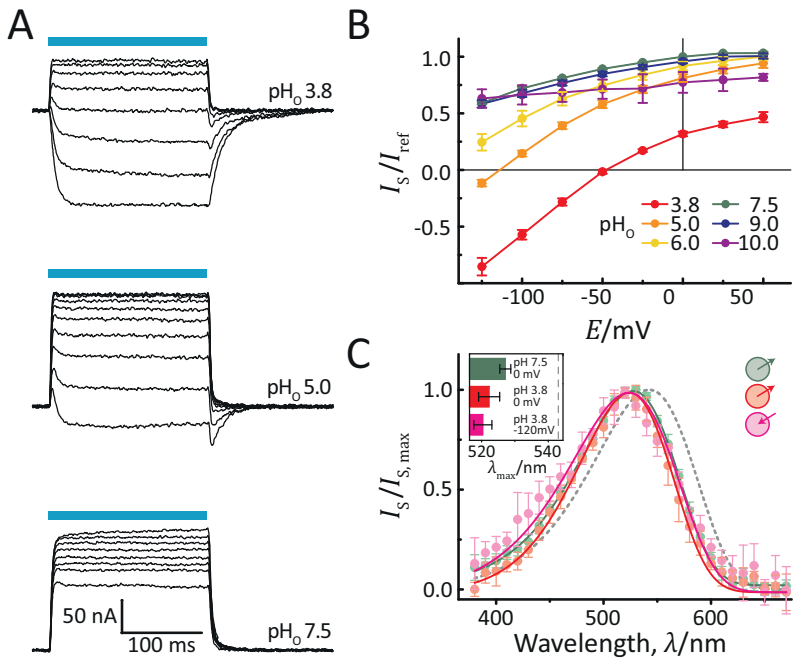

Figure S2. Characterization of GR-H87A.
The conserved Histidine residue was exchanged by Alanine to prevent potential coupling with the Schiff base counterion D121. A. Typical photocurrents at different extracellular pH conditions and holding voltages ranging from -125 mV to +75 mV. Stationary outward and inward directed currents are maintained whereby transient peak currents disappeared. Measurements were carried out under identical conditions as GR-H87M (Fig. 2 B-D). Even though, for photoactivation cyan light of 500±25 nm was used. This observation supports the conclusion that the conserved His87 is not crucial for inward currents. B. *I(E)*-Plot of stationary currents of GR-H87A with similar characteristics like GR-H87M as already mentioned before (Fig. 2C) (mean ± SE, n ≥ 6). C. Action spectra show a blue shift of about 16 nm compared to GR-WT (Fig. 1D). A distinct pH and voltage dependent difference could be not observed similar to GR-WT. The pH/voltage-dependence of GR-H87M might be a specific feature of the replacement by Methionine (Fig. 2D). (mean ± SD, n ≥ 6)

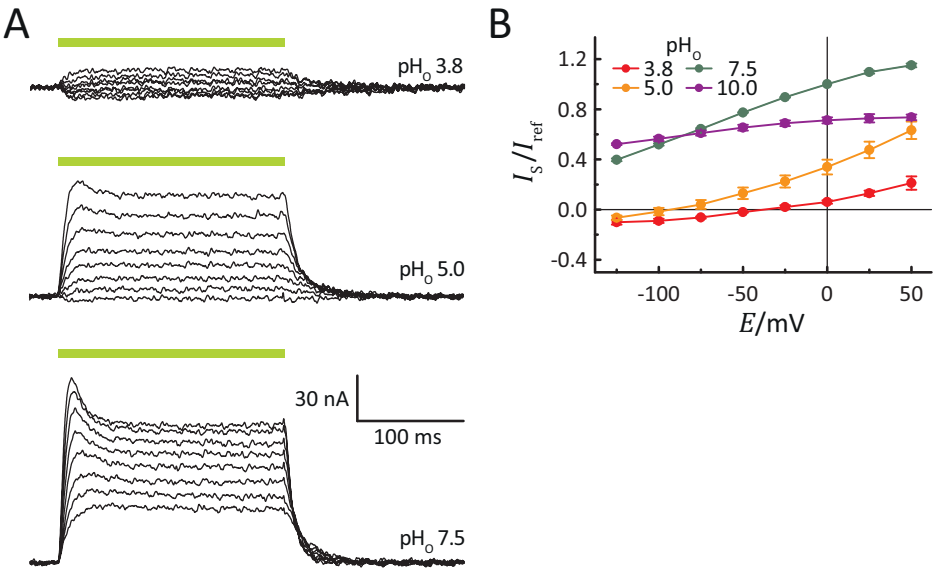

Figure S3. Characterization of GR-S77C.
A. Photocurrents were measured in oocytes similarly as for GR-E132D and GR-S77A (Fig. 3) at holding potentials between -125 mV and +75 mV. The currents showed similar characteristics as the other two mutants although replacement of S77 by cysteine is a conservative exchange. B. $I(E)$-Plot of stationary currents of GR-S77C (mean ± SE, n=4).

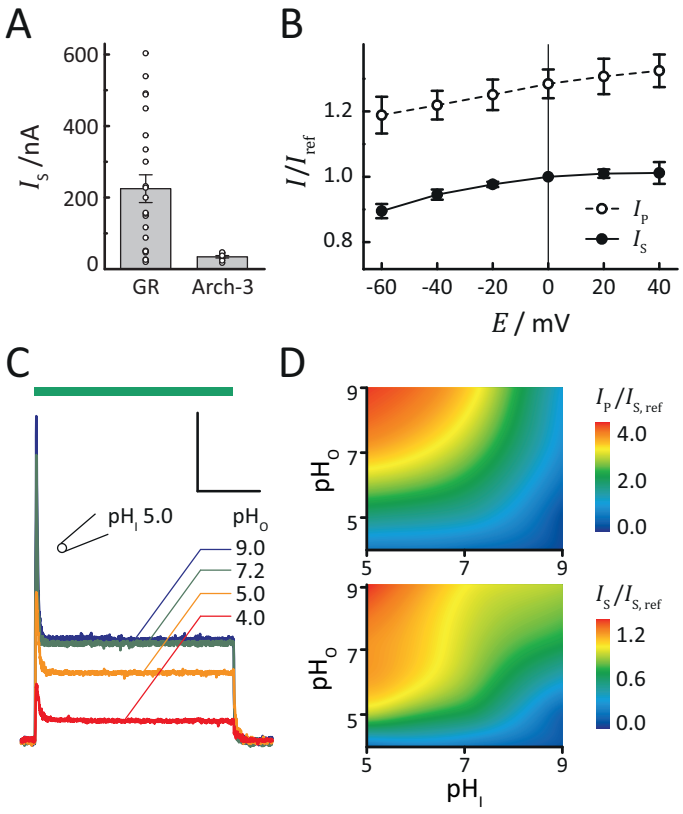

Figure S4. Whole-cell measurements of GR-WT-expressing HEK-293 cells.
A. Comparison of stationary photocurrent amplitudes (mean ± SE) of GR (n=23, 540±7 nm) and Arch-3 (n=9, 565±7 nm) at a holding voltage of 0 mV. Photocurrents of GR were about five fold higher compared to Arch-3. B. *I*(*E*)-plot of peak and stationary currents of GR-WT at pH_o 7.2 (n=8) normalized to stationary photocurrent at 0 mV. Current-voltage relation is similar to oocyte measurements (see Fig. 1B). C. Photocurrent traces of GR-WT expressing HEK-293 cell at different pH_o while the intracellular pH_i was 5.0, measured at 0 mV holding potential. Scale bar: 70 pA, 50 ms. The photocurrent amplitudes decrease with increasing extracellular proton concentrations as expected for a proton pump. D. Peak and stationary currents at various pH_o (4.0, 5.0, 7.2 and 9.0) as well as different pH_i (5.0, 7.2 and 9.0). The holding potential was kept at 0 mV (n=3 for each pH_o/pH_i pair). Data points between measured values are linearly interpolated. Photocurrents were normalized to the stationary current at symmetric proton concentrations (pH_o=pH_i).

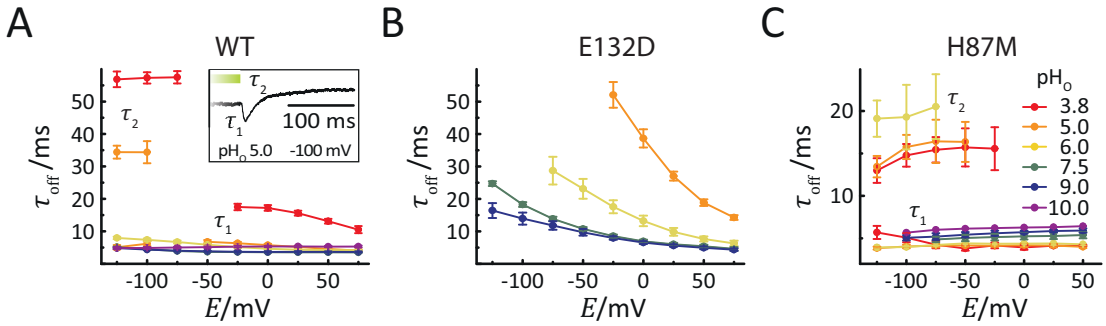

Figure S5. Kinetic properties of GR-WT, GR-E132D and GR-H87M
Characteristics of τ_{off} for GR-WT (A), GR-E132D (B) and GR-H87M (C) at different pH$_o$-values and holding voltages. The inset (A) shows biphasic kinetic decay at low pH$_e$ where τ_1 corresponds to a fast off-kinetics of the active pump mechanism and τ_2 refers to the kinetic of the passive inward proton flux. For determination of kinetic parameters only current amplitudes with $I_S \geq 60$ nA were analyzed (mean ± SE, n ≥ 9 (WT), n ≥ 6 (E132D), n ≥ 6 (H87M)).